Empirical correlator for stochastic local CD uniformity in extreme ultraviolet lithography

Peter De Bisschop[a,*] and Steven G. Hansen[b]

^aIMEC, Leuven, Belgium
^bASML Technology Development Center, Chandler, Arizona, United States

Abstract. We present experimental evidence for an empirical correlator (or model) for stochastic local CD uniformity (LCDU) of contact holes printed in resist with 0.33-NA EUV lithography. The key component of this correlator is a term that has the "traditional" inverse proportionality to the image log-slope (ILS). We also show that, when the contact CD is close to (one of) the stochastic pattern-failure cliffs (i.e., missing contacts or merging contacts), additional terms need to be added. These terms represent the steep rise in LCDU that is typically observed in the vicinity of these cliffs. We also demonstrate an approach for generating the image-intensity function from which ILS is calculated to obtain the best LCDU correlation result (a procedure which we call "image calibration"). Several experimental LCDU data sets that support the validity of the proposed correlator are presented. © *2022 Society of Photo-Optical Instrumentation Engineers (SPIE)* [DOI: 10.1117/1.JMM.21.3.033201]

Keywords: stochastics; EUV; contact holes; local CD uniformity; correlator; empirical model; image log-slope; pattern-failure cliffs.

Paper 22015G received Apr. 15, 2022; accepted for publication Jul. 26, 2022; published online Aug. 8, 2022.

1 Introduction

Critical dimension uniformity (CDU) has always been an important metric of any lithographic process, and in EUV lithography, it is even more so due to the importance of stochastic effects on local CD-variability. In the case of contact printing, this local CD-variability is quantified by local CDU (LCDU), which is defined as three times the standard deviation of contact CDs measured within a small area in the die. Stochastic effects are not the only contributor to LCDU. CD variability on the mask and measurement noise also play a role, but in EUVL, stochastic effects are at least a major and often the dominant contributor. This is why stochastic LCDU has been the subject of both experimental and theoretical studies in the past decades, aiming at a better understanding and—if possible—prediction of how LCDU varies with target structure, exposure conditions, and process conditions.

Very early on in this type of work, the link between stochastic CD variability and the quality of the optical image (in resist) was made: an improved image quality leads to a smaller stochastic CD variability. Image quality can be quantified by several metrics, but usually image-log slope (ILS) or normalized ILS (NILS ≡ CD × ILS) have been put forward as the most relevant ones. Several theoretical models for describing stochastic CD variability, in which ILS or NILS occur,[1–11] have been proposed, and several experimental correlation studies also supported this dependency.[9,11–18] However, the published experimental LCDU correlations do not make it entirely clear whether ILS or NILS is the most appropriate metric to describe the image quality impact on LCDU. If LCDU data are collected for structures that print mean CD values that are very close, ILS and NILS are equivalent parameters, but information about the mean CD range of the published experimental data is not always available. So, the question of whether the best parameter to correlate to LCDU is ILS or NILS, in our opinion, has not yet been answered satisfactorily, nor is it clear whether a unique answer exists or whether different experimental cases correlate to different image metrics.

*Address all correspondence to Peter De Bisschop, peter.debisschop@imec.be

In this paper, we study this question by looking into a few (extensive) data sets, obtained from different resists and exposure conditions and covering a CD range (per mask structure) that in some cases extends significantly beyond the CD variation in a normal process window. We show that the key correlator to stochastic LCDU can be written as $CD^n \times ILS$, where n is a number that takes a value between 0 and 1, depending on the data set used. Some of the data sets presented here show the best correlation if we set $n = 0$, which means that ILS is the relevant image metric. In a case in which $n = 1$, NILS is the better metric for describing the image-quality impact on LCDU, and we also show a case in which an n value in between appears to be the best choice. (We also outline a metrology-related argument that makes the presence of such a CD^n term plausible in Appendix C.)

Our results also show that this $CD^n \times ILS$ term alone cannot explain all of the LCDU data in our measurements, and we demonstrate that the LCDU correlator needs to be extended with additional terms, if the mean CD is close to the stochastic printing-failure cliffs (i.e., the missing-contact cliff or the merging-contact cliff).[17,19,20] We call these additional terms the "cliff terms." So, in its most general form, the LCDU dependency on image quality and mean CD is written as

$$LCDU = A\frac{1000}{CD^nILS} + B + CliffTerms(CD). \tag{1}$$

The functional form that these CliffTerms can take is detailed later. In a normal yielding process, in which the mean CD is "far enough" from the stochastic failure cliffs, these CliffTerms are very small to negligible, but we show how Eq. (1) makes it possible to describe the steep increase in LCDU that is often observed experimentally when the CD is close to one of the cliffs (or perhaps even to both, in the case of very tight pitches).

We present Eq. (1) as an empirical correlator to (or predictor for) experimental LCDU data, which means that A, B, and n (as well as the model parameters that appear in the cliff terms) are to be fitted to experimental LCDU data. Its purpose should then be to use it as an LCDU predictor for structures or conditions that are not included in the data set that was used to fit the model. It is important, however, to be clear that Eq. (1) can only be used to predict how LCDU varies with dose, focus, CD, pitch, mask bias, and illumination mode, at a fixed resist and resist/underlayer process. If the resist or process is changed, we believe that the model form of Eq. (1) should still be valid, but the model parameters $(A, B, n, \ldots)$ will be different. This places the scope of the model in Eq. (1) within the realm of OPC/SMO type of predictions. Indeed, given the increasing importance of having a good LCDU control over the entire chip, OPC- or SMO-type software packages now must have the ability to do a full-chip verification of LCDU [or line width roughness/line edge roughness (LWR/LER) in an L/S-type application], throughout the intended process window, for a fixed resist process. This requires a predictor that is fast and accurate enough to cover variations in mask structure (e.g., pitch, mask bias), focus and dose, and (in the case of an SMO-type software) illumination mode. We found that Eq. (1) largely meets this goal in the experimental cases included in this paper, as well as in several other data sets (not included here) that the authors have studied over the past years.

In Sec. 2, we describe the experimental cases of this paper, specify the metrology used to measure LCDU, and give the approach we developed to generate the image-intensity function from which we calculate ILS (an approach we call "image calibration"). In Sec. 3, we apply Eq. (1) to each of these data sets and discuss our findings. Section 4 summarizes our work and its conclusions.

2 Description of the Data Sets and Experimental Conditions and Procedure

2.1 Experimental LCDU Data Sets

Table 1 summarizes the LCDU data sets included in this paper. All wafers were exposed on a 0.33-NA EUV scanner at imec and cover several resists (from different vendors) and illumination modes. (The illumination modes used are shown in Figure 1.) Each data set contains LCDU

Table 1 Experimental data sets discussed in this paper.

Data set	Resist	Underlayer	Wafer type	Contact grid type; pitch range	Illumination source shape
1	PTD-CAR 1 (vendor 1)	Organic	FEM	Square grid; 42 to 80 nm	SMO
2	PTD-CAR 1 (vendor 1)	Organic	Dose-meander	Square grid; 42 to 60 nm	SMO
3	PTD-CAR 2 (vendor 2)	SOG	FEM	Square grid; 38 to 76 nm	Quasar
			FEM	Hexagonal grid; X70Y40 to X84Y48	Hexapole
4	Spin-on MOR	SOG	FEM	Square grid: 38 to 76 nm	Quasar
5 (Appendix)	PTD-CAR 3 (vendor 1)	Organic	Dose-meander	Square grid: 38 to 90 nm	Quasar
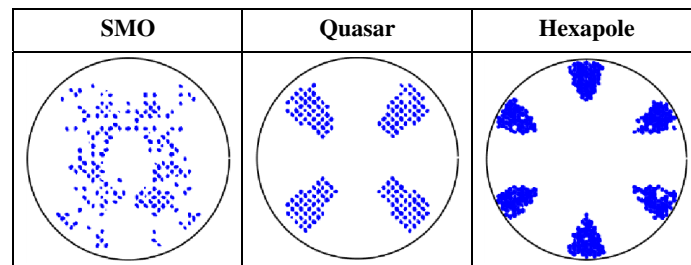
Fig. 1 Illumination modes.

data from contacts placed on either a square grid or a hexagonal grid at multiple pitches. All LCDU values were measured from resist wafers; no etch step was applied.

We included both positive-tone development chemically amplified resists (PTD-CAR), from two different vendors, and a spin-on metal-oxide resist (MOR). The illumination modes that we used include an SMO source that was optimized for a via layer of one of the logic test vehicles at imec, as well as more standard quasar- and hexapole-type sources. We used FEM wafers to generate LCDU data through focus and dose and dose-meander wafers (varying dose at a single focus) in cases in which we wanted to generate LCDU data over a very large dose (and hence CD) range. Data set 3 consists of two wafers, exposed with the same resist, but one exposed with a quasar source and the other with a hexagonal source. The goal of combining two (very) different illuminations is to check whether a single correlator of the type of Eq. (1) can simultaneously fit to the LCDU data from both illumination modes. An LCDU correlator (or predictor) that is used in an SMO context would need to have that capability. Combining two very different source shapes in a single data set makes a severe test on its illumination mode independence.

2.2 Wafer Metrology

The CD-SEM images were measured on a CG5000 or CG6300 Hitachi CD-SEM, and the contact CD values were subsequently generated from those images using Hitachi's DGA+ software. The CD values that we use in this work are the (average) CD-diameter, obtained from an elliptical fit of the contact resist edge [see Fig. 2(a)], using a 60% threshold edge-detection algorithm. Each LCDU value reported in this work is the 3σ variation around the mean CD, obtained from between 1000 and 2000 individual CD values (measured from four to eight images with a field-of-view (FOV) of 1125 nm and a pixel side on 1.1 nm/pixel), depending on the pitch.
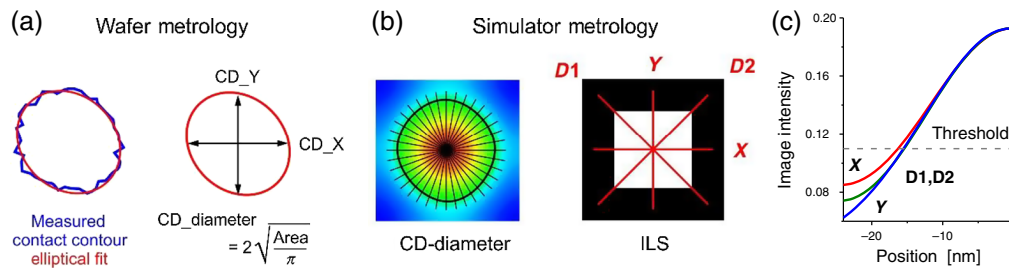
Fig. 2 Illustration of contract-metrology metrics: (a) on wafer and (b) in the simulator. On wafer, we use the CD_diameter metric, which is derived from the area of an ellipse (red), fitted through the resist-edge contour (blue). The simulator "wagon wheel" CD is generated in a comparable way, by evaluating the image-in-resist intensity at many metrology lines. For the calculation of ILS, we used the average ILS value calculated at four metrology lines: *X*, *Y* and two diagonal metrology lines, *D*1 and *D*2. (c) An example of the image along three metrology lines for the case of a 48-nm pitch square contact array, exposed with the SMO illumination mode of Table 1. The ILS is clearly not the same along these metrology lines.

2.3 *Simulator Metrology: Which ILS?*

The key metric in Eq. (1) that represents the optical image quality is ILS, but in the case of a contact hole, we need to decide how we want to calculate ILS. This parameter is related to a one-dimensional cut through the two-dimensional image-intensity (a metrology line), and selecting a different orientation of this cut will in general result in a different ILS value. As we are using the CD-diameter wafer-metrology choice, a choice that is not related to any specific metrology line through the contact hole but essentially includes all possible metrology lines through the center of the hole, it seems logical to do something similar when calculating ILS: calculate ILS for several metrology lines and use the average value for application in Eq. (1). In practice, we calculate ILS along the *X*- and *Y*-directions and the two diagonal directions, as shown in Fig. 2(b):

$$\text{ILS} \equiv \text{Mean}(\text{ILS}_X, \text{ILS}_Y, \text{ILS}_{D1}, \text{ILS}_{D2}). \tag{2}$$

Figure 2(c) shows the example of the aerial-image intensity of a 48-nm pitch contact along the horizontal, vertical, and diagonal metrology lines. It is clear that the slope of the image intensity (i.e., ILS) along each of these metrology lines but at a common intensity threshold is different.

Including additional metrology lines should in principle improve the average ILS value, but from the result of our correlations it would seem that taking just these four cuts was enough for the cases that we studied.

The contact CD that we take from the simulator is the so-called "CD-diameter," which is derived from the positions along a large series of metrology lines where the image-in-resist (calculated in a selected plane in the resist, parallel to the resist surface) equals a specified threshold value. This metric is comparable to the wafer CD_diameter.

All of the simulations for the study in this paper were done with Prolith2020b using the "Maxwell accelerated" mask calculation, solving the mask-diffraction equations at multiple sampling points for each source.

2.4 *Image-Calibration Procedure*

This section describes the procedure that we use to generate the image intensity and the intensity threshold from which we calculate ILS for correlation to LCDU. This procedure—we call it "image calibration"—consists of several steps. In each of these, one or more simulation parameters are optimized to best "align" the wafer measurements and the image calculations. This procedure is shown in Fig. 3. Each of the steps is explained in the sections that follow.
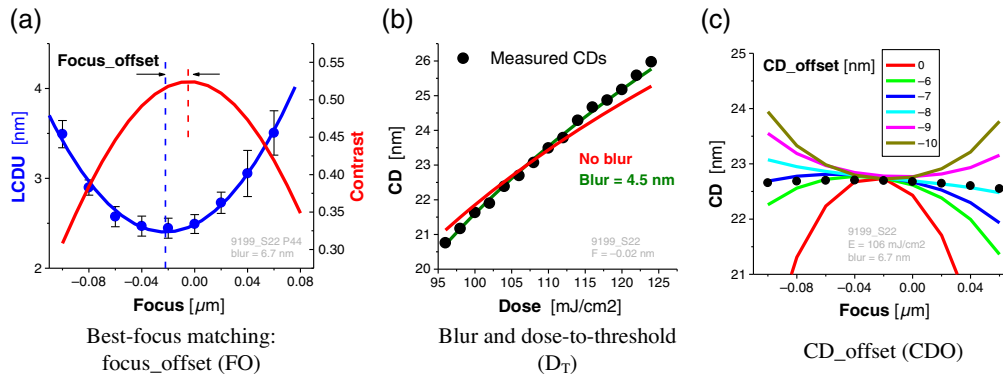
Fig. 3 Illustration of the different steps in the image-calibration procedure that we use to calculate the images from which ILS will be derived. (a) Best-focus matching: FO, (b) blur to dose-to-threshold (D_T), and (c) CD_offset (CDO).

2.4.1 *Focus-offset calibration*

Whenever doing simulations that are to be compared with wafer data, it is necessary to determine the offset between the focus scales in the simulator and in the scanner, as there is in general an arbitrary delta between them. For the sake of LCDU correlations, we take this a step further and do a separate "focus matching" for each mask structure[20] included in the LCDU data set. Mask three-dimensional (3D induced focus shifts between structures can be substantial in EUVL, and there often is a residual difference between the measured and simulated best focus through-pitch dependency. Such residuals in the focus-scale matching have a negative impact on the correlation quality. We therefore relate scanner- and wafer-focus scale for each structure j separately as

$$\text{Wafer\_best\_focus}(j) - \text{wafer\_focus} = \text{Simulator\_best\_focus}(j) - \text{simulator\_focus.} \quad (3)$$

In this equation, we calculate the best focus values as follows:

$$\text{Wafer\_best\_focus} = \text{minimum}(\text{LCDU}(\text{focus})), \quad (4a)$$

$$\text{Simulator\_best\_focus} = \text{maximum}(\text{Contrast}(\text{focus})). \quad (4b)$$

(The minimum and maximum values are obtained as the extrema of a polynomial fit through the data. Note that the simulator best focus could equally well be calculated from the variation of ILS or NILS through focus.) Figure 3(a) shows an example. The variation of this focus offset parameter, FO (≡ Wafer_best_focus - Simulator_best_focus), through the various structures included in our data sets usually stays within ±10 nm [see example in Fig. 4(a)], but we found that correcting for such effects improves the wafer-to-model match. This is equivalent to saying that the best-focus prediction accuracy of the simulation engine used for LCDU predictions should be as high as possible.

Figures 4(b) and 4(c) show the usefulness of the optimization of the Focus_offset parameter. The LCDU (focus) and ILS (focus) comparison in Fig. 4(b) shows a focus-mismatch of ~10 nm. If uncorrected for, the LCDU-ILS correlation in Fig. 4(b) shows a "V-shape" (red curve). Correcting for this focus offset (green curve) places the data much better on a single curve.

2.4.2 *Calibration of the image blur and dose-to-threshold scale*

Rather than calculating ILS from the optical-only image, it is often calculated from a blurred optical image,[10] in which the blur is a simplified representation of the resist impact. Such a blurred image can be easily calculated as follows. Most lithography simulators offer the option to convolve the optical image with what is called a "vibration" or "noise" function; this is what we use to blur the image. We typically use a Gaussian blur function, characterized by a single parameter, which we will call the "blur parameter." The amount of blur that needs to be included

(a) Measured and simulated best-focus values vs. pitch. (with offset between averages removed)

(b) Illustration of the application of the CD_offset parameter to align LCDU(focus) to ILS(focus)

(c) Demonstration of a 10 nm focus mismatch between LCDU and ILS: the correlation data shows a characteristic "tilted-V shape"
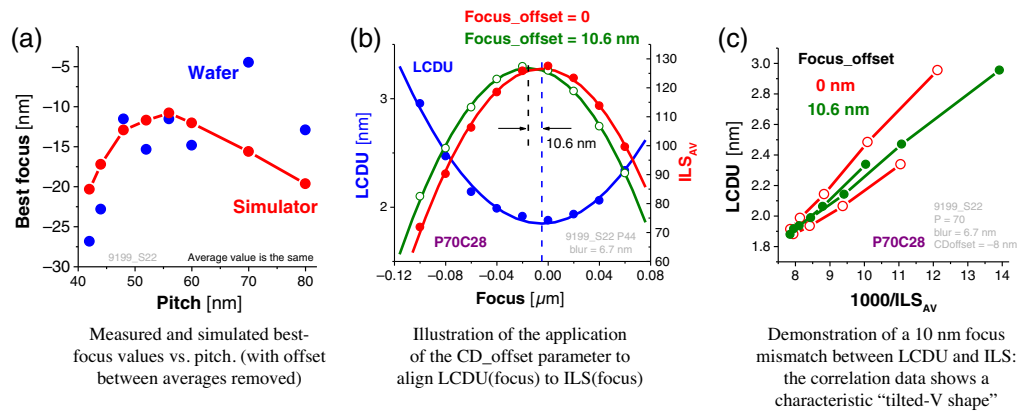
Fig. 4 Illustration of the need and usefulness of optimizing the Focus_offset parameter for each mask structure of the data set. (Example taken from data set 1 of Table 1.) (a) Measured and simulated best-focus values versus pitch (with offset between averages removed). (b) Illustration of the application of the CD_offset parameter to align LCDU (focus) to ILS (focus). (c) Demonstration of a 10-nm focus mismatch between LCDU and ILS: the correlation data show a characteristic "tilted-V shape."

in the simulator can be estimated by matching the measured CD (dose) dependency with the simulated CD (threshold) dependency, where dose and threshold are assumed to be inversely proportional:

$$\text{Threshold} = \frac{D_T}{\text{dose}}. \qquad (5)$$

D_T is a parameter that we fit to the measured data for each mask structure independently. Figure 3(b) illustrates how, using the appropriate values for blur and D_T, we can usually match measured CD (dose) dependencies quite accurately.

In this work, we use a common blur parameter for all of the mask structures included in the same LCDU correlation experiment. When we use ILS in this paper, it always refers to this "blurred ILS."[10]

2.4.3 *Calibrating CD_offset (CDO), to match the CD (focus) dependency*

The two previous steps in the image calibration (or an equivalent approach) are fairly common, but when only those two steps are done, the CD (focus) dependency obtained from the wafer and from the simulator can be quite different, especially when doing measurements close to the iso-focal CD of a structure. The resist chemistry shifts the position of the isofocal CD from where it lies in a purely optical model (blur alone does not shift the isofocal CD much), and we found that our LCDU correlations significantly improve if we add a third step to the image calibration. In this step, we calculate the value of a CD_offset (CDO) parameter, such that CD_simulator +CD_offset has the same focus dependency as CD_wafer. Figure 3(c) shows an example in which the optimum CDO value is −7 nm. In this example, we applied this procedure to the through-focus CD data from a single exposure dose, but when our experimental data set consists of FEM data, we optimize the value of CDO on the full Bossung and include the CD data from all of the mask structures in the data set. This means that we use a CDO value that is the same for all mask structures. In Appendix A, we show an example that demonstrates how much the use of a well-optimized CDO parameter can improve the LCDU-ILS correlation.

By applying this procedure, we do not pretend that the value of CDO corresponds to a real CD-metrology "error." Rather, we take it as an additional fitting parameter in our LCDU model because we find that we obtain a better agreement between simulated ILS and measured LCDU data if we apply this CDO parameter to match the CD (focus) dependency between wafer and simulator.

Table 2 Summary of the model parameters that are optimized during the image-calibration procedure.

Model parameter	Goal	Constant or structure dependent	Remarks
Focus_offset (FO)	Match simulator best focus to wafer best focus	Structure dependent	Requires through-focus data. If not available, FO = 0 is a reasonable choice.
Dose-to-threshold conversion parameter, D_T	Calculate image threshold value for each dose value	Structure dependent	—
Blur	Match CD (dose) dependency	Constant	—
CD_offset (CDO)	Match CD (focus) dependency	Constant	Requires through-focus data. If not available, CDO = 0 is a reasonable choice

2.4.4 *Summary of the fitting parameters in our image-calibration procedure*

We end this section with a table (Table 2) that summarizes the model parameters that are optimized in our image-calibration procedure and mark explicitly which of these parameters are constant over all structures contained in the LCDU data set and which parameters we adjust separately for every mask structure (e.g., pitch). As with any OPC-type model, when we change to a different data set using a different resist process, the image calibration procedure needs to be done again. So, all of the parameters in Table 2 will in principle change when going to a new data set. Variations on the approach outlined in this section are possible of course.

3 Correlation Results

We now discuss the LCDU-correlation results of data sets 1 to 4 of Table 1. Each of these data sets adds some new learning about this type of correlation. Together, they demonstrate that the LCDU correlator that we constructed is reasonably successful in covering the variation of LCDU through focus, dose, mask structure (i.e., pitch and mask bias), and illumination mode at a fixed resist process. It is, however, not perfect, and we will also show an example in which not all of the data fit into a single correlation. (The correlation results of data set 5 are found in Appendix B.)

3.1 *Data Set 1: PTD-CAR Resist FEM Data (SMO Source)*

This data set consists of what we think is the baseline data set for the type of LCDU correlation that we are investigating in this paper: CD- and LCDU-Bossung data for a set of different mask structures. In this case, the mask structures are all square contacts on a square grid, with pitches varying from 42 to 80 nm. With the SMO source that we used to print these structures, 42 nm is very close to the practical resolution limit, i.e., the pitch where the two printing-failure cliffs are so close together that there is (almost) no failure-free CD window left.[17,19,20] At 80 nm pitch, the contacts are optically isolated. Figure 5 shows an example of the CD- and LCDU Bossungs for two of the pitches. The lines in the CD Bossung plots correspond to the Prolith-simulated CD values obtained after optimizing the parameters of the image-calibration procedure.

Table 3 contains some details of the results of the image-calibration procedure, as an illustration of the type of parameter values that we obtained in this case.

With the parameters from the image-calibration now known, we calculated the average ILS [according to Eq. (2)], for each point of this data set, using Eqs. (3) and (5) to convert the wafer focus and dose into the corresponding simulator focus and threshold. This finally gives us the data for the LCDU-ILS correlation; see Fig. 6.

We find that the simple correlator of Eq. (1), but without any CliffTerms, gives an excellent result, with $n = 0$ being the best choice (i.e., there is no need for a CD term in the correlator).
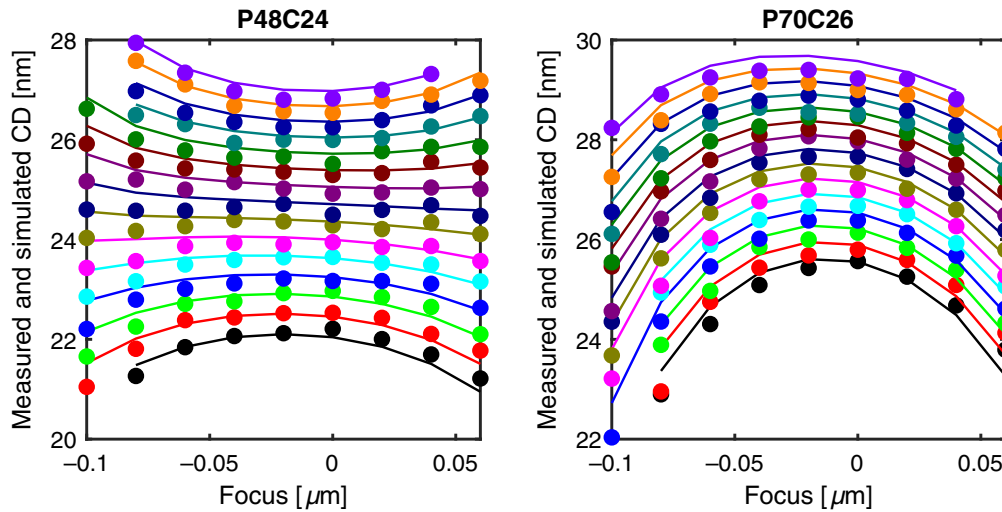
Fig. 5 Example of the measured (symbols) and the simulated (lines) CD-Bossungs, after application of the image-calibration procedure, for two pitches of data set 1. The agreement of both dose- and focus-dependencies is excellent in these examples.

Table 3 Summary of image-calibration parameters obtained with this data set. A structure code such as P42C25 means that pitch and nominal mask CD are 42 and 25 nm, respectively (at 1X). This table shows a typical example of the amount of through-pitch variation of the parameters D_T and FO. The second last line of the table contains the rms of the CD difference between measured and simulated Bossung (always after the image calibration): the agreement is excellent for each of the eight pitches. The last line has the value of the Pearson R correlation coefficient of a linear fit per pitch through the LCDU (1000/ILS) data. (See also Fig. 6).

Parameter	Value							
Blur (nm)	6.7							
CDO (nm)	−8							
Structure	P42C25	P44C25	P48C26	P52C26	P56C27	P60C27	P70C28	P80C28
D_T (mJ/cm^2)	11.3	11.3	11.2	11	11	10.9	10.7	10.5
FO (nm)	12	12	5	10	7	9	−5	−1
CD rms (nm)	0.24	0.29	0.21	0.32	0.22	0.29	0.30	0.25
R coeff. of LCDU correlation	0.86	0.925	0.979	0.966	0.993	0.988	0.987	0.979

3.2 *Data Set 2: PTD-CAR Resist Dose-Meander Data (SMO Source)*

This second data set uses the same resist, process conditions, and illumination mode as data set 1, the only difference is that these data are measured from a dose meander wafer (exposed at a constant focus). This allows us to generate LCDU data for a much larger CD-range than what was available on the FEM wafer. In a normal application, the dose/CD range that the correlator should cover is much smaller than the range in the current data set 2, but the goal of trying this larger dose/CD range is to generate a more severe test on the simple 1/ILS correlator. We find that the simple 1/ILS correlator is not sufficient anymore, as Fig. 7 shows.

As the process of this data set 2 is identical to the process of data set 1 (and the two wafers from which they were measured were exposed at the same time), one could expect that the correlator that we obtained from data set 1 should also be consistent with the results of data set 2. But Fig. 7 shows that this is not the case. The symbols in Figs. 7(b) and 7(c) are the measured
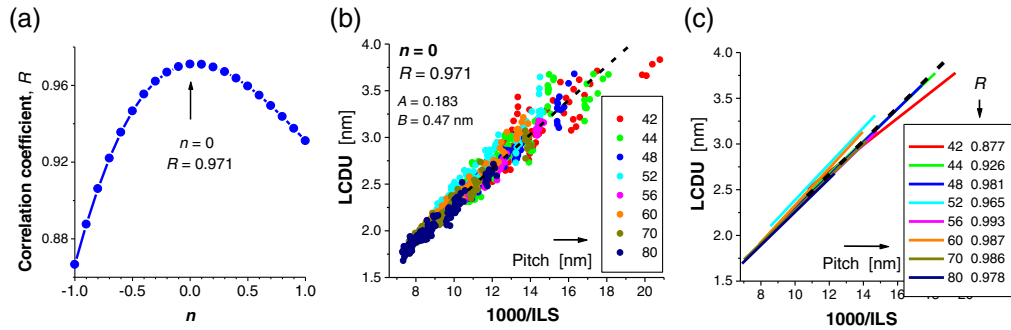
Fig. 6 LCDU-ILS correlation results for data set 1. (a) A value of $n = 0$ gives us the best correlation coefficient. (b) The correlation plots including all individual data points, almost 1000 points. The black dashed line is a linear fit through the data. (c) The result of a linear fit through the data of each individual pitch, together with the fit through all of the data. All of the individual pitches except pitch 42 nm follow the overall linear fit line very nicely. Table 3 lists the correlation coefficient R per pitch. Except for the smallest two pitches, all R values are >0.96.
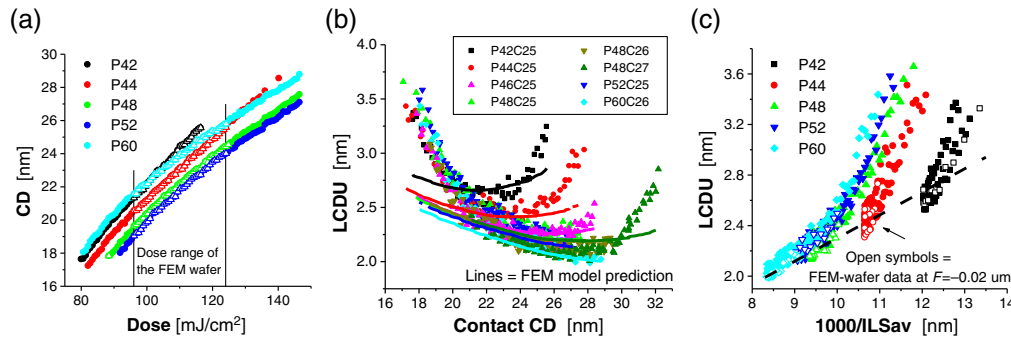
Fig. 7 (a) The dose/CD range of the five pitches in this data set. The open symbols mark the dose range of the FEM wafer of data set 1. (b) The measured LCDU (CD) data. The symbols are the measured data, the lines the prediction form the correlator obtained in data set 1. (c) The LCDU-ILS correlation plot. The black line corresponds to the best fit from data set 1 (black-dashed lines in Fig. 6). It is clear that the FEM-data model does not describe this new data at all.

LCDU data, and the lines are the LCDU prediction using the correlator that we fitted from data set 1. It is clear that this model only agrees with the measured data in a limited CD range, corresponding more or less with the CD range that was available on the FEM wafer. Both at the smaller and larger CD sides, the new data deviates considerably from the previous model prediction.

We can see what is happening if we measure the upper part of the pattern-failure cliffs (from the same dose-meander wafer). Figure 8 shows this for the example of pitch 48 nm. As long as the stochastic failure probabilities are below $\sim 10^{-6}$ to 10^{-9} (our data do not give us an exact number), the LCDU data follow the simple 1/ILS model [i.e., the solid lines in Fig. 8(a)], but when the CD comes close to either of the stochastic-failure cliffs, LCDU values increase. This should not be surprising: if the impact of stochastics becomes large enough to create pattern failures, it seems obvious that CD-variability should be affected as well. However, the simple 1/ILS model does not predict this effect.

It must be noted right away that a process with failure probabilities $> \sim 10^{-6}$ to 10^{-9} would probably not be a yielding process, and hence there is no need for an accurate LCDU prediction. But for the sake of demonstrating that the deviation of LCDU from the simple 1/ILS behavior that we observe in this data set is indeed linked to the failure cliffs, we extended the 1/ILS LCDU correlator with two extra CD-dependent terms, which we call the "cliff terms":
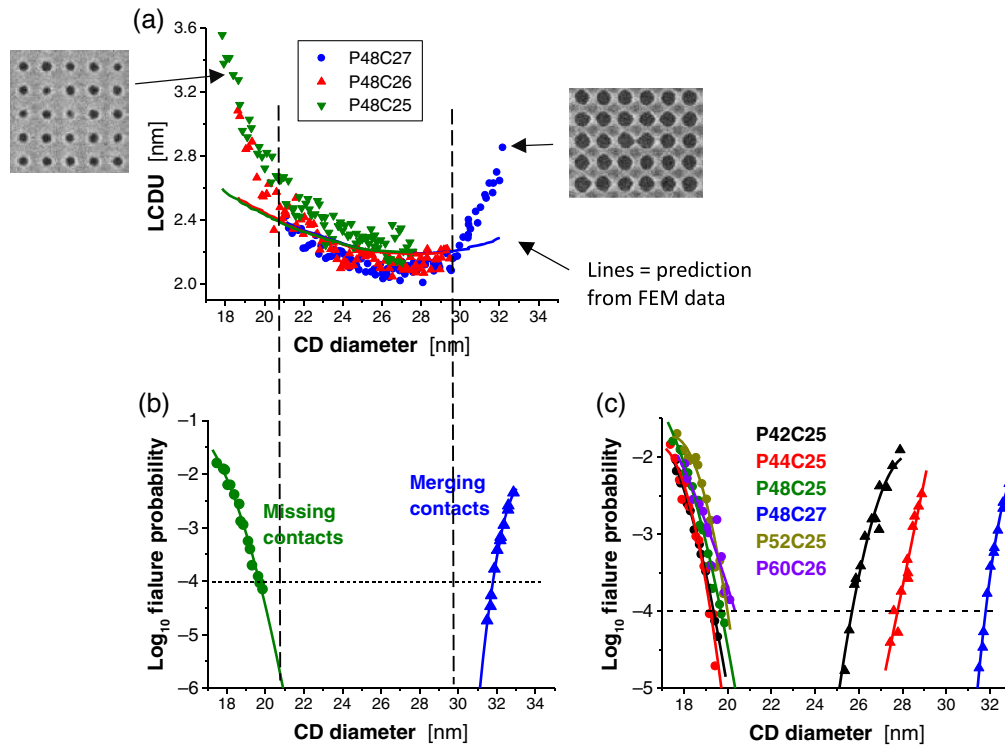
Fig. 8 (a) Measured LCDU (CD) and (b) measured failure probabilities. When the failure probability exceeds a certain value, LCDU increases above the values predicted by the simple 1/ILS model. (Note that we combined the data from three different mask biases to generate this result.) (c) The upper part of the failure cliffs for all of the structures of this data set. These data are used to estimate the cliff-position values, cd_0 and cd_1, of Eq. (6).

$$\text{LCDU} = A\frac{1000}{CD^n\text{ILS}} + B + A_1\left(\exp\left(-\frac{\text{CD}-\text{cd}_0}{t}\right) + \exp\left(\frac{\text{CD}-\text{cd}_1}{t}\right)\right). \qquad (6)$$

The first exponential term in Eq. (6) represents the LCDU increase at the missing-contact cliff side (the "missing-contact" cliff term"), and the second represents the LCDU increase at the merging-contact cliff side (the "merging-contact cliff term"). We chose to use an exponential form for these cliff terms, mainly because the failure probability cliffs approximatively have an exponential dependency on CD, but any other function that has a fast increase with increasing/decreasing CD would probably work as well. We gave both cliff terms a common amplitude (A_1) and decay constant (t) as this appears to work sufficiently well. This also limits the number of additional model parameters to be fitted to the data, but different values could of course be used for the two cliff terms if necessary.

The cd_0 and cd_1 parameters in Eq. (6) require specific attention. These represent the "positions" of the missing-contact cliff and merging-contact cliff, respectively, and these positions are in general different for every structure (i.e., pitch, in the current experiment). Rather than treating cd_0 and cd_1 for each pitch as an individual fit parameter, we derive it from an approximate measurement of the failure cliffs, shown in Fig. 7(c). These cliffs were obtained from CD-SEM images and hence represent the upper part of the cliffs only, but for the sake of our argument in this section, this proved to be sufficient. From the data in Fig. 7(c), we derived the CD-value at which the missing-contact failure probability is 10^{-3}, a somewhat arbitrary choice, but given the limited dynamic range of the cliff data, we could not reliably extrapolate it to much smaller values. If we call these CD values $cd_{\text{missing}}(P)$, we chose to set the values of cd_0 and cd_1 as follows:

$$\text{cd}_0(P) = \text{cd}_{\text{missing}}(P) + \text{CD}_0, \qquad (7a)$$

$$cd_1(P) \approx P\text{--}CD_1, \tag{7b}$$

where CD_0 and CD_1 are constant (i.e., pitch independent) parameters that we will treat as fitting parameters in our LCDU model. With the parameter CD_0, we make it possible for $cd_0(P)$ to take a value that is different from the CD at which the missing contact probability is 10^{-3} (which was, as we said, an arbitrary choice in the definition of $cd_{missing}$). The equation that we use for $cd_1(P)$ essentially says that we expect contacts to start merging when the width of the resist separating them approximately equals CD_1. This is an approximation, but as most of the data in this data set are relatively far away from the merging-contact cliffs, it turns out to be sufficient.

The extended model of Eq. (6) therefore contains in total seven model parameters that we use to fit to the measured LCDU data: A, B, A_1, t, CD_0, CD_1, and n. The correlation result that we obtained after optimization of these parameters is shown in Fig. 9(b). We show the measured LCDU (CD) data for each pitch individually, together with the result of the LCDU prediction from Eq. (6). Also shown is the improved correlation plot for the data from all pitches [Fig. 9(a)]. If we compare this with the initial correlation with the simple 1/ILS correlator in Fig. 7(c), it is clear that adding the cliff terms greatly improves the result.

In Appendix B, we show a similar result for a more extensive data set (data set 5 of Table 1), obtained from a different resist and illumination mode, containing data from more pitches. The result is equally convincing, which adds to the evidence that the cliff terms are a relevant extension to the simple ILS model.

Once again, we want to emphasize that the cliff terms in Eq. (6) can be ignored if all of the CDs in the application are sufficiently far from the stochastic-failure cliffs (which is expected to be the case if the process is to have yield). But we believe that the cliff terms can describe many of the observed cases in which LCDU does not appear to follow the expected 1/ILS behavior. Dense contacts in particular are sensitive to this as the two cliffs are relatively close to each other. The cliff terms are also critical when generating accurate LCDU models for small pitch and small CD contacts, which are often the main focus of advanced litho process development. (The LCDU data for pitch 42 nm in data set 1, i.e., the FEM data set, are in fact already somewhat affected by the cliffs terms, which is why its correlation is worse than for the other pitches.)
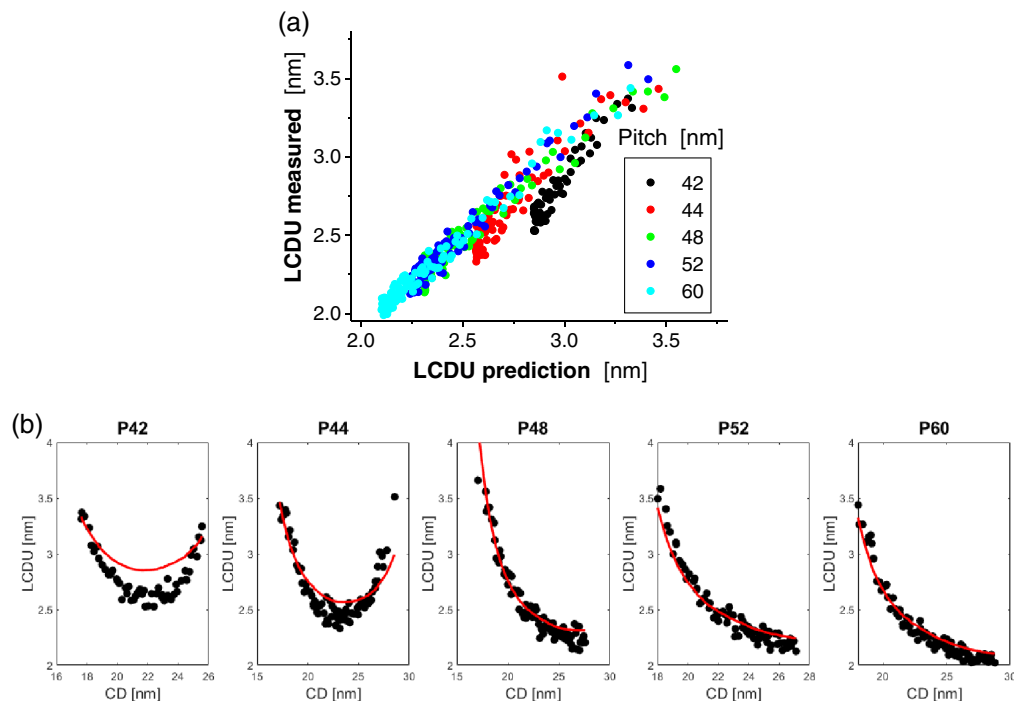

Fig. 9 Result of the fit of data set 2 to the LCDU correlator of Eq. (6), for each of the five pitches of this data set. The value of the pitch is labeled of top of each LCDU(CD) plots. The model fit parameters that we obtained are $A = 0.192$, $B = 0.5$ nm, $A_1 = 1.28$ nm, $t = 1.57$ nm, $CD_0 = -3$ nm, $CD_1 = 13$ nm, and $n = 0$.

In generating the next two data sets, we paid attention to keeping a sufficient distance from the failure cliffs.

3.3 Data Set 3: PTD-CAR Resist FEM Data, Exposed with Two Different Sources

Apart from using a different PTD-CAR resist from a different resist vendor, this data set adds a new element to the correlator test in that it contains data from two different illumination modes. It is important to test whether the correlator holds when the source changes, if the correlator is to be applicable to SMO. If this is indeed the case, the correlator covers any change in the optical image caused by a change in dose, focus, pitch, mask bias, or illumination mode.

To make this source-dependency test a severe one, we chose two very different source shapes: a quasar-type source and a hexapole-type source. These were used to expose contacts on a square grid and on a hexagonal grid, respectively. We first look at the correlation of these two subsets separately and then combine them into a single data set.

Figure 10, first of all, illustrates these two subsets. The CD- and LCDU-Bossung examples demonstrate the low noise level that we achieved in our experiments, something which is important when evaluating different correlation options.

3.3.1 Hexagonal-grid contacts exposed with the hexapole source

When performing the image calibration on the hexagonal-grid contact LCDU data only (exposed with the hexapole source), we observe something that we have not seen before in the other data sets (see key results in Fig. 11): the optimum n parameter is not zero, even though at $n = 0$, the correlation is still very good. The correlation quality when taking the LCDU data of each individual pitch separately has almost no dependency on n, but in the combined correlation (as in Fig. 11), the data from all pitches combined align just a little better if n is close to 0.5.

3.3.2 Square-grid contacts exposed with the quasar source

We obtain a similar result when making the correlation plots for the square-grid contact LCDU data only (exposed with the quasar source): including the CD^n term in the correlation does not change the correlation quality for each pitch taken separately, but if we correlate the data from all pitches together, we find a clear nonzero n optimum. The n-optimum is not very sharp: the linear

(a)

(b)

Contacts on a hexagonal grid. pitch combinations include (P_X, P_Y): (70,40), (73,42), (80,46) and (84, 48)

Contacts on a square grid. pitch combinations include: 38, 40, 42, 46, 48, 50, 54, 64, 68 and 76 nm
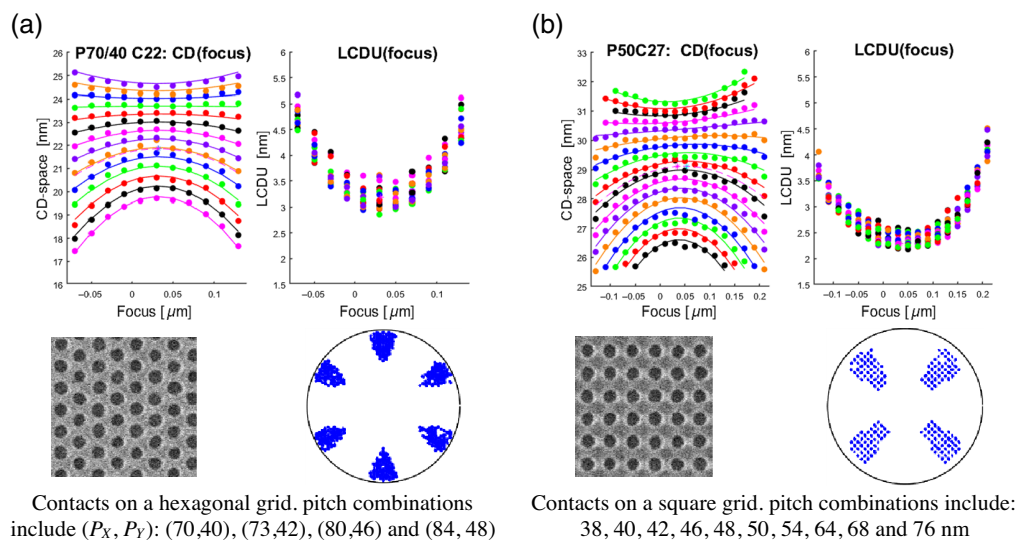
Fig. 10 Illustration of the two contact-grid types included in data set 3. The top row shows a CD- and LCDU Bossung example for each grid type: the symbols are the measured values, and the lines are a functional fit (so, not simulated data) through the measured data.
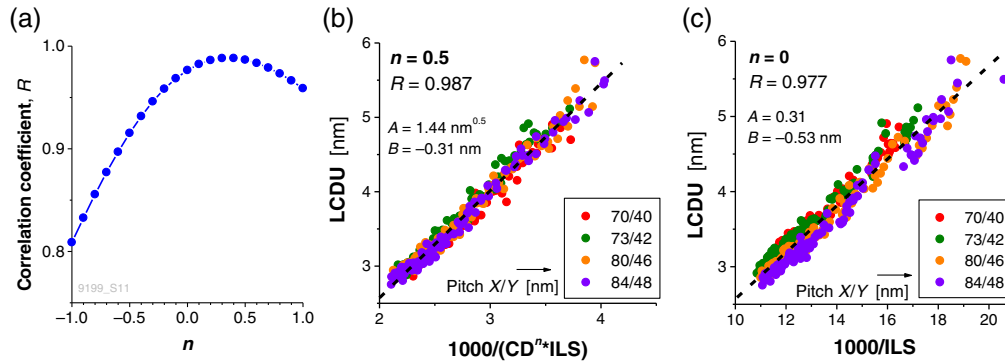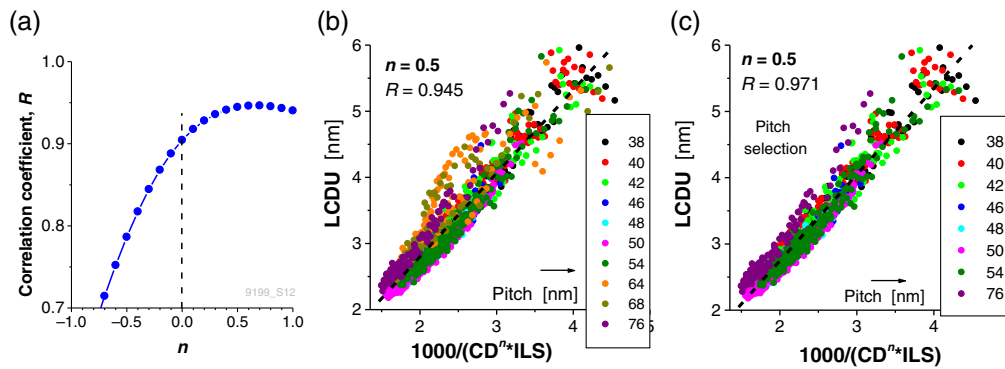
Fig. 11 LCDU-ILS correlation for the hexagonal-grid contact data only. The optimum values for blur and CDO are 6 and −2.5 nm, respectively. (a) We find the best correlation (i.e., the highest value of the Pearson correlation coefficient R when doing a linear fit) around $n = 0.5$, but the optimum is not very pronounced: R is larger than 0.97 for all n values from 0 to 0.8. This can be seen by comparing plots (b) and (c), which are the correlation plots for $n = 0.5$ and $n = 0$, respectively.

Fig. 12 LCDU-ILS correlation for the square-grid contact data only. The optimum values for blur and CDO are 6 and −3.5 nm, respectively. Plot (a) shows $R(n)$; it has its maximum around $n = 0.4$. The correlation plot in (b) includes all of the measured pitches, and pitches 64 and 68 nm are left out in (c).

correlation coefficient R is >0.94 for all n-values between 0.4 and 1, but below $n = 0.4$, the R value drops rapidly, as shown in Fig. 12. For the correlation plots in Fig. 12, we chose to use $n = 0.5$ (as we find that this is the best value when correlating the LCDU value from the square-grid and hexagonal-grid contacts together, in Sec. 3.3.3).

The LCDU correlation further improves if we leave out the data from two pitches, 64 and 68 nm. These are the first two pitches for which a higher diffraction order starts entering the lens pupil, i.e., they are what are sometimes called forbidden pitches. Their process window is smaller than for the other pitches, and we also found that the measured versus simulated $CD(E, F)$ agreement (after image calibration) is not as good as for the other pitches. Why forbidden-pitch cases should have a weaker LCDU correlation is not entirely clear. We speculate that resist profiles may be less well defined, leading to less robust metrology. With a smaller process window, it can also be expected that the impact of the failure cliffs is not negligible. The mask that we used for this data set did not provide enough measurement area to measure these cliffs, but in an earlier paper,[20] we measured the missing-contact cliff from another resist but exposed with essentially the same illumination mode, and we found that the missing-contact cliffs for pitches 56 to 62 nm occur at larger contact CDs than the missing-contact cliffs of either smaller or larger pitches. We see that data set 4, which is exposed at the same illumination mode as data set 3, also shows deviating correlation behavior for pitches 64 and 68 nm. This confirms that the cause of this behavior at these pitches is linked to the particular quasar illumination mode used for these two data sets.
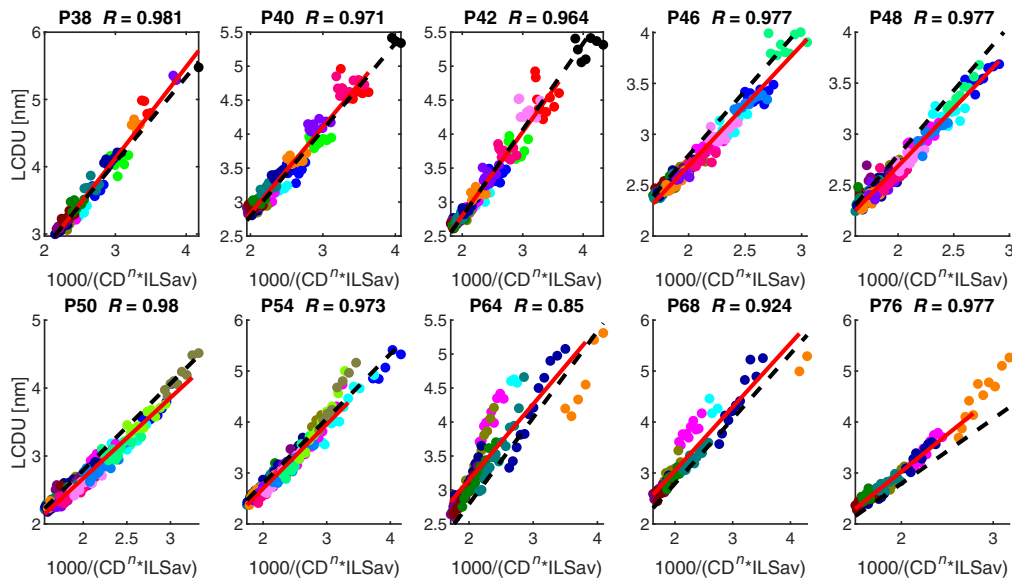
Fig. 13 Individual pitch correlation for the square-grid contact cases of data set 3. The red lines are a linear fit to the data of each individual pitch (with the Pearson correlation coefficient R given in the title); the black-dashed line is the linear fit though the data from all pitches together. Data points belonging to a common defocus were given the same color. The highest LCDU values correspond to the most-out-of-focus positions.

The LCDU data per pitch in Fig. 13 shows more clearly the excellent correlation for all pitches, except these two deviating cases.

3.3.3 Hexapole and quasar data combined

Finally, we make a joint correlation of all of the data in this set, i.e., we combine the hexagonal-grid from the hexapole-exposed wafer and square grid data from the quasar-exposed wafer in a single LCDU model fit. All of the data except pitches 64 and 68 nm of the square-grid subset are used; we leave those out here to better see the joint correlation of the pitches from both data subsets. First, we fine-tuned the image calibration on this combined CD-LCDU data set, leading to an optimum at blur = 6.5 nm, CDO = −3.5 nm, and $n \approx 0.5$ nm (though the n-optimum is again not very sharp: for all n values from 0.4 to 0.7 the linear correlation coefficient R is larger than 0.97).

Figure 14 shows the resulting correlation plot for all of these pitches together, and Fig. 15 plots the result for each pitch separately. In both cases, the black dashed line is the linear fit through all of the data, and the colored lines in Fig. 15 are a linear fit to the data of each individual pitch.

Different colors in each of the plots in Fig. 15 correspond to data from a different defocus. At the lower LCDU side, the data follow the linear fit line very closely. The higher-LCDU data show a larger spread around the fitted line, but this corresponds to the data from the most out-of-focus conditions. Having a model that is somewhat less accurate at these extreme defocus positions is probably not such an issue. Another remark is that we ensured that the data points (at least in best focus) were not too close to the pattern failure cliffs, but we could not check that for all data points. So, there may be some impact of the cliff terms at the out-of-focus data points, especially for the densest pitches, where the two cliffs are not too far apart from each other. The wider spread of the data around the linear fit at the larger LCDU side (data points that are most out-of-focus) is likely to be due to the contribution of the cliff terms.

The main conclusion from the results of this data set is that a single correlator is indeed capable of covering LCDU data obtained from different illumination sources and can hence be used within an SMO context.
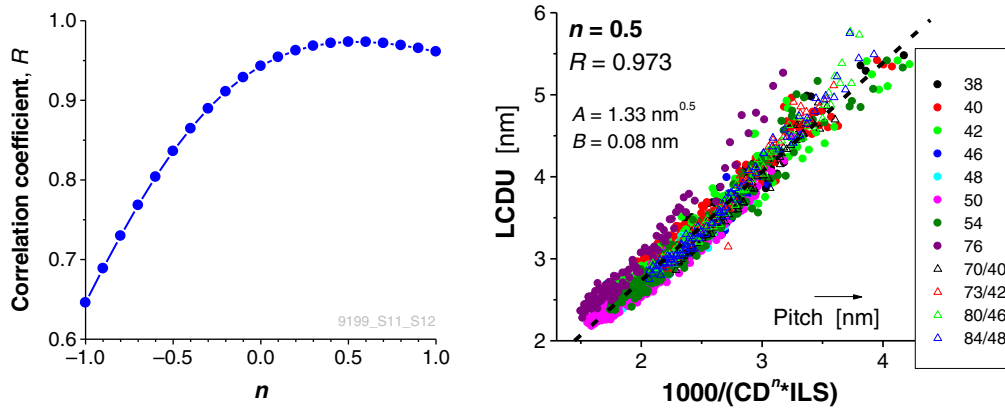
Fig. 14 Results of the correlation of the square-grid contact and hexagonal-grid contact together. (CDO = −3.5 nm, blur = 6.5 nm.) The data from the hexagonal-grid contacts are plotted as open triangles. The joint correlation is very convincing.
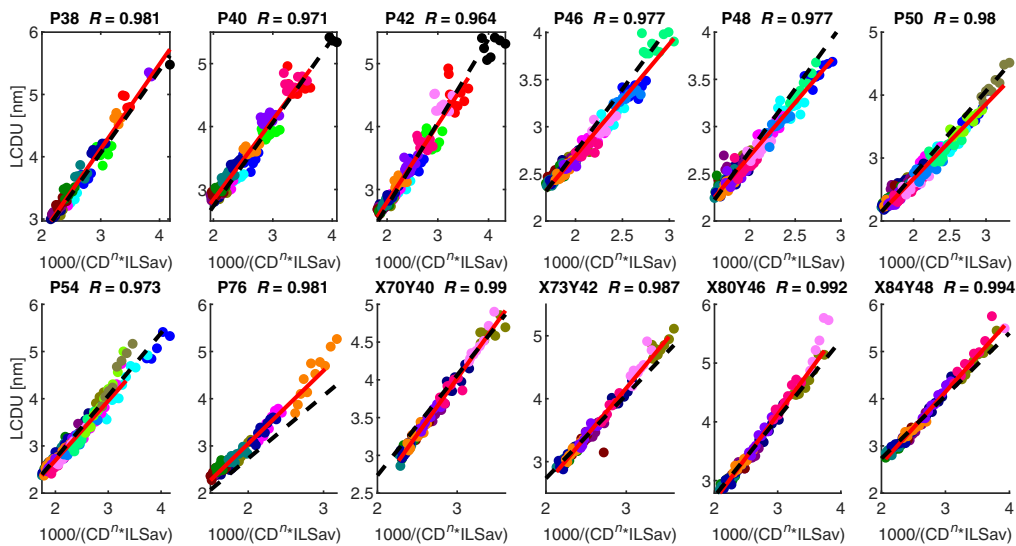

Fig. 15 Fit to the LCDU data for each pitch separately (red line); the black dashed line is the fit through the complete data set (from Fig. 14). Data points with a different color correspond to a different defocus.

3.4 *Data Set 4: Resist Dots Printed with a Spin-on Metal-Oxide Resist*

Data set 4 consists of CD-LCDU data of dot patterns on a square grid, printed with a spin-on MOR resist and exposed using the same illumination mode as the one we used for data set 3 (quasar source). CD values are the "outer diameter" CD, following an elliptical fit of the resist edge. As in the previous data set, we measured CD-LCDU-Bossungs for pitches 38 to 76 nm.

The image calibration procedure was the same as the one used for the other data sets and yielded best values for blur and CD-offset of 2.5 and −2 nm, respectively. The lower value of the blur is expected: the operation of an MOR resist does not rely on diffusion mechanisms, but it has been reported to have a small but nonzero blur.[21] The result of our image calibration is consistent with this.

The LCDU correlation has an R-coefficient larger than 0.95 for any n value from 0.8 to 1.3. This means that LCDU approximately correlates with 1/NILS and not 1/ILS, a conclusion that is consistent with an LCDU correlation that we published earlier[17] on an older MOR resist. Figure 16 shows the result of the correlation of all of the LCDU values of this data set.
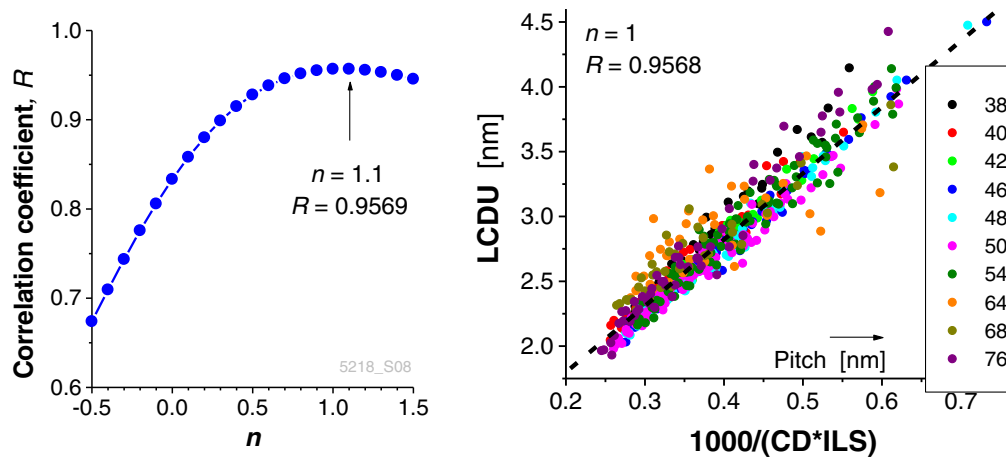
Fig. 16 Correlation of MOR resist LCDU data. In this case, correlating LCDU to ($n = 1$) turns out to be the better choice.
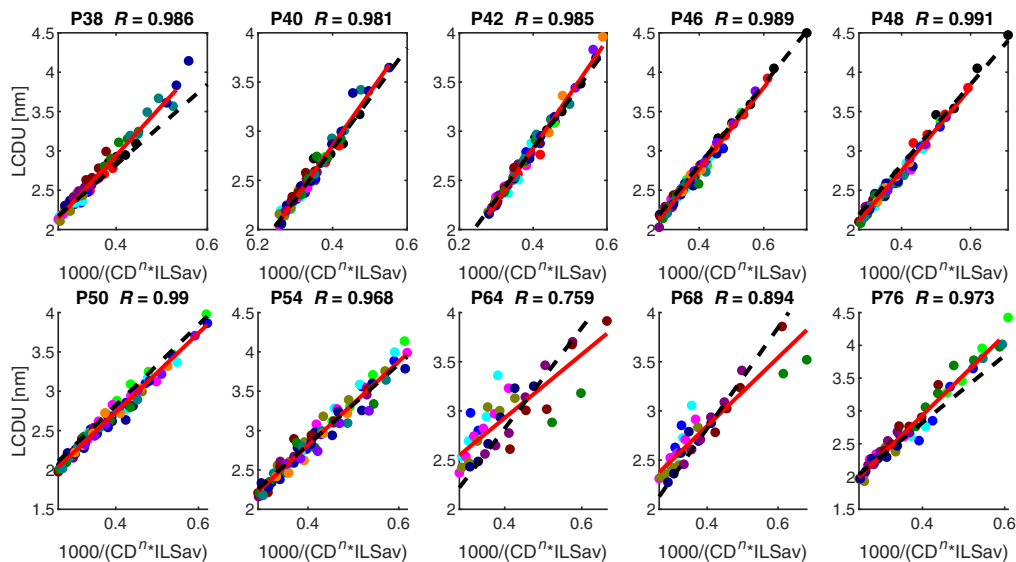

Fig. 17 Fit to the LCDU data for each pitch separately (red line); the black dashed line is the fit through the complete data set (from Fig. 16). Data points with a different color correspond to a different defocus.

Again, we find an excellent correlation, although – as in data set 3—pitches 64 and 68 nm fit less well, as shown in Fig. 17. This strengthens our hypothesis, expressed in the previous section, that pitches in the forbidden-pitch region fit less well to our correlator due to a less robust metrology (resist-edge detection), an increased impact of the cliff terms, or both. The main conclusion from this data set remains, however, that our basic LCDU correlator works equally well for an MOR resist as for the PTD-CAR resists that we have tested.

4 Discussion and Summary

This paper presents a selection of the EUVL LCDU data sets, obtained from resist wafers, that were analyzed by the authors over the past couple of years. The goal of this study was to see whether it is possible to find a functional form for an empirical LCDU correlator that works for all of the data that we have looked at. The purpose of such a correlator (or predictor) is that, once

it is calibrated on measured LCDU data obtained from a given resist process, it can be used as a predictor for the LCDU of contact configurations that were not measured. We see the usefulness of such a predictor primarily in an OPC/SMO context, which means that the correlator/predictor should cover variations in focus, dose, pattern type (pitch, mask size, and contact configuration), and illumination mode, at a fixed resist process. To be practically useful, it must be fast enough for full-chip applications. This is why we favor an empirical correlator that depends only on quantities that can be efficiently calculated from the image-in-resist (or from the aerial image).

All of the data that we have shown in this paper (as well as data from several other data sets that we did not include here) were found to be consistent with a simple correlator that contains the following elements: ILS, CD, and stochastic-cliff-related terms [see Eqs. (1) and (6)]. The cliff terms are only non-negligible when the CD of the contact is close to one of the stochastic-failure cliffs (missing or merging contacts). We estimated that these cliff terms are negligible when the stochastic failure probability is smaller than 10^{-9} to 10^{-6}. Although these numbers are a rough estimate only, they carry a message. For advanced logic-type applications, nearly all of the vias must print to get yield, which means that failure probabilities would have to be below the 10^{-12} level.[22] Memory applications can probably accept somewhat larger via-failure probabilities, but in general one can assume that the cliff terms can be ignored in the case of a yielding process. A lot of research work close to the resolution limit is currently being done, however (e.g., in the context of resist-screening or process development), where yield is not yet a major consideration. In such circumstances, one can run into situations in which the observed LCDU trends can only be understood when the cliff terms are taken into account, as our study has shown (Sec. 3.2 and Appendix B).

It is interesting to speculate whether this observation could be turned around: Can we obtain useful information about the (approximate) stochastic-failure cliff positions simply by measuring around which CD the measured LCDU data starts deviating from the expected 1/ILS dependency? Measuring stochastic-failure cliffs is time consuming (if they need to be done with e-beam based metrology); LCDU measurements are much faster. It does not seem likely that we can retrieve the full cliff from LCDU data, but if LCDU measurements could be used to locate the 10^{-6} failure probability CD (to take an example), that could save time, especially if this measurement would be done for multiple contact-pitches or contact configurations. Such an LCDU-based method, applied to multiple structures, could be helpful in calibrating failure-prediction models.

When the cliff terms are negligible, we find that LCDU correlates linearly with $1/(\text{CD}^n\text{ILS})$:

$$\text{LCDU} = A\frac{1000}{\text{CD}^n\text{ILS}} + B. \tag{8}$$

We initially included the CD^n term because the existing literature often relates LCDU to NILS, which corresponds with $n = 1$. So, we used n as a fitting parameter and, for each data set and looked for which value resulted in the best correlation. The data sets that we have presented in this study led to various values of n, ranging from $n = 0$ to $n = 1$. It is interesting to speculate from where these differences might come, but we have no good explanation at present. Appendix C describes a metrology-related argument leading to an expected $\text{CD}^{0.5}$ term in the correlator. Although our data sets show a more varied behavior, this argument does make the (valid) point that the way we measure contact CD and hence LCDU can be expected to have an impact on the correlator that the data require. We speculate that differences in contact-edge roughness or resist profile could also lead to differences in the best correlator from one resist to another.

With respect to metrology, we also made the point in the beginning of the paper that it is important to align wafer metrology to simulator metrology as much as possible. In our work, we used the CD-diameter metrology both on the wafer and in the simulator. This means that the CD is derived from a large number of resist-edge detection points obtained along many metrology lines, passing through the center of the contact from different directions. Consequently, we also use an ILS that is averaged over multiple metrology lines for our correlations. In principle, one could make a different choice, for example, measure the contact CD along the X-axis or along the Y-axis. In that case, it is logical to correlate to the ILS along the corresponding metrology line.

We tried this on some of our data sets but found the quality of the correlation to be worse than in the case in which the CD_diameter and average ILS values are used. We think that this is related to the fact that *X*- or *Y*-CDs measured from a wafer are not simply obtained as an *X*- or *Y*-cut through the measured resist contour but are derived from an elliptical fit of the complete contour of the contact, which makes them somewhat dependent on the complete contact shape. Also, we found that *X*- and *Y*-CDs measured on wafers are noisier than the CD-diameter values (and often show a correlation between CDx and CDy in practical data sets).

Another important element for obtaining a good correlation is to calculate ILS from what we call a "calibrated image." The image-calibration procedure that we outlined in Sec. 2 consists of four elements:

1. The wafer-simulator focus scale is adjusted for each individual mask structure in the data set. This leads to a structure-dependent focus-offset (FO) parameter that we obtained by matching the measured LCDU (focus) to the simulated contrast (focus) or ILS (focus) dependency. Even FO values no larger than ~10 nm, when not corrected for, have a clear impact on the correlation quality. This observation implies that any simulation engine that would use a correlator like the one that we propose must have a very accurate mask 3D engine to make correct prediction of the structure-dependent focus shifts. It is also possible that the need for optimizing such an FO parameter in the calibration procedure handles (at least to some extent) offsets between how a simulator calculates a CD and the details on how wafer measurements convert a 3D resist structure into a single CD value.

2. A resist blur parameter is optimized to match the CD (dose) dependency between wafer and simulator. The use of such a blur in resist-image-only (or aerial-image-only) simulations, e.g., mimic the diffusions processes that take place in a CAR resist, is in fact fairly common.[10]

3. Equally important is to apply a CD_offset (CDO) between measured and simulated CDs, to match the CD (focus) dependencies for each structure. The example in Appendix A shows what happens if no such CD offset is applied: the correlation does not disappear completely, but it does become clearly worse. We do not claim that the CD-offset values that we optimized from our data sets correspond to an actual metrology error. We prefer to see it as an additional empirical parameter in our correlation approach that we found to be helpful.

4. The dose-to-threshold conversion is adjusted for each mask structure separately, with the threshold being proportional to 1/dose. This amounts to a form of empirical OPC for matching CD through pitch (or pattern).

Even though we obtained good results with the correlator presented in this paper and with the approach that we developed to calculate it, we are certain that experimental cases may exist in which it does not work as well. In other words, we do not claim our correlator is perfect, and more work is likely to lead to further improvements or will lead to a better understanding of its limitations.

We mentioned a few times that we see the use of the correlator that we discussed in the paper as a model in an OPC/SMO context. In that sense, our paper has discussed the "model calibration" step only but has not really addressed the question of how accurate the model is when used to predict the LCDU for structures or conditions that are not included in the calibration data set. Such an evaluation of the accuracy of the correlator would be called the "model verification" step. We acknowledge that such a verification step is a necessity before the correlator can be used for making actual full-chip predictions. We must leave this next step to future work, however.

A final word about etch. All our LCDU data are obtained from resist wafers, but in the final product contacts will be etched, and it has been demonstrated that etch changes the LCDU values.[22] To what extent our empirical correlator would still be usable to match to post-etch LCDU variations with focus, dose, mask structure, and illumination mode is a question that we have not included in this study. We acknowledge that it is an important question, but must leave it to future studies to find its answer.

5 Appendix A. Correlation for Data Set 1 with Only Partial Image Calibration

In Sec. 3.1, we showed a good LCDU correlation result for data set 1, being FEM data from a wafer exposed with an SMO-type source. To achieve this result, we performed the image-calibration procedure of Sec. 2.4. What we want to show in this appendix is what happens if the CD_offset (CDO) calibration part is left out, i.e., if we put CDO = 0 nm. A recalibration of the blur parameter at CDO = 0 nm gives an optimum value of 4 nm. After repeating the Focus_offset (FO) and dose-to-threshold (D_T) calibrations, the best LCDU-ILS correlation is shown in Fig. 18. Compare this result with Fig. 6, where the CDO parameter also was optimized.
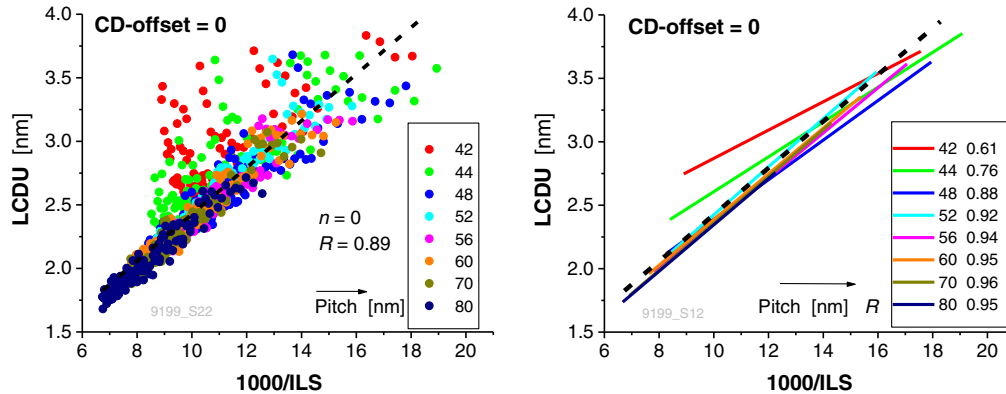
Fig. 18 LCDU-ILS correlation result of data set 1 when the image calibration procedure is done with a fixed CDO value of 0 nm. The result is clearly worse than what we obtain when CDO is also optimized (see Fig. 6).

Especially for structures with the close-to-isofocal CD Bossung (i.e., the denser pitches) is the difference large: without application of a CD-offset, the simulated CD (focus) dependency differs significantly from the measured dependency. The LCDU-ILS correlation for these pitches is then also very poor. Leaving out the CDO calibration has much less (to almost no) effect on the more isolated pitches: the LCDU-ILS correlation for the individual pitches is good, and they are consistent with the correlation of the full data set. This comparison illustrates the usefulness of the CDO-parameter optimization for near-isofocal structures.

Note, however, that if an LCDU data set does not contain any through-focus data, the value of CDO is found to be of much less impact and can in fact be set to zero.

6 Appendix B. Data Set 5 Results

Data set 5 (see Table 1) provides a second example in which the cliff terms in the LCDU correlator of Eqs. (1) and (6) prove their usefulness. This data set is generated from a different resist-illumination mode combination than data set 2, and it contains more pitches. These pitches range from 38 to 90 nm, and for every pitch, LCDU data were taken at three to four different mask biases (similar to the example shown in Fig. 11 of Ref. 17).

This data set has no through-focus data, which means that the CD_offset (CDO) term cannot be determined by the image-calibration approach of Sec. 2.4.3. But a data set in which the CDs only vary through pitch and dose can still be matched quite well if we take CDO = 0 nm, so this is what we did. The optimum blur value for this case was 6 nm.

The upper part of the missing-contact cliff could be measured for all pitches of this data set, giving us the $cd_{missing}(P)$ dependency of Eq. (7a), where we (somewhat arbitrarily) took $cd_{missing}$ as the CD for which the measured missing-contact probability is 10^{-3} (this value is
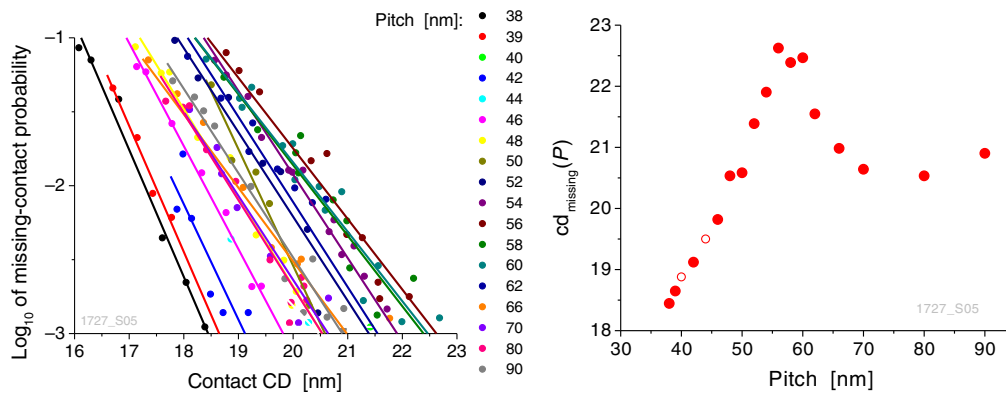
Fig. 19 Measured missing-contact probabilities for the pitches included in data set 5, and the $cd_{missing}(P)$ function that was derived from it, as the cd for which the missing-contact probability is 10^{-3}.

an ~arbitrary choice, but taking a high value means that inspecting a small wafer area is sufficient to obtain these data). Figure 19 shows the measured missing-contact cliffs (the high missing-probability part of the cliff only) and the $cd_{missing}(P)$ function that was derived from it.

We fixed the parameter t in the cliff terms to the value that we previously found in data set 1 ($t = 1.57$) and fixed $n = 0$. This left us with five model parameters to be fitted: A, B, A_1, CD_0, and CD_1.

To demonstrate the usefulness of the cliff terms in the correlator again, we fitted two models to data set 5: one with the cliff terms [Eq. (6)] and one without [Eq. (8)]. Figure 20 compares the correlation result for both models. It is again clear that the cliff terms greatly improve the overall correlation. We present the comparison between the two models in a different form in Fig. 21, by plotting LCDU versus CD for each pitch separately. The blue and black lines in these plots correspond to the prediction from the LCDU model without and with cliff terms, respectively. One difference between the two that is obvious from this comparison is that, with the basic ILS model of Eq. (8), LCDU decreases with increasing CD. The presence of the cliff terms can make LCDU increase again at the large CD side, which is indeed what we see in the experimental data.
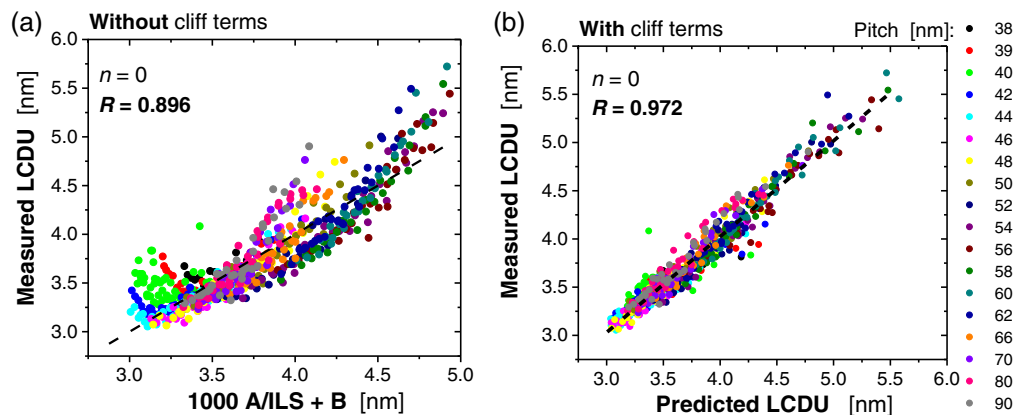

Fig. 20 Comparison of the LCDU correlation result of data set 5 using a model (a) without and (b) with the cliff terms. The difference between the two needs no further comments. (CDO = 0 nm, $n = 0$, and blur = 6 nm in both models).
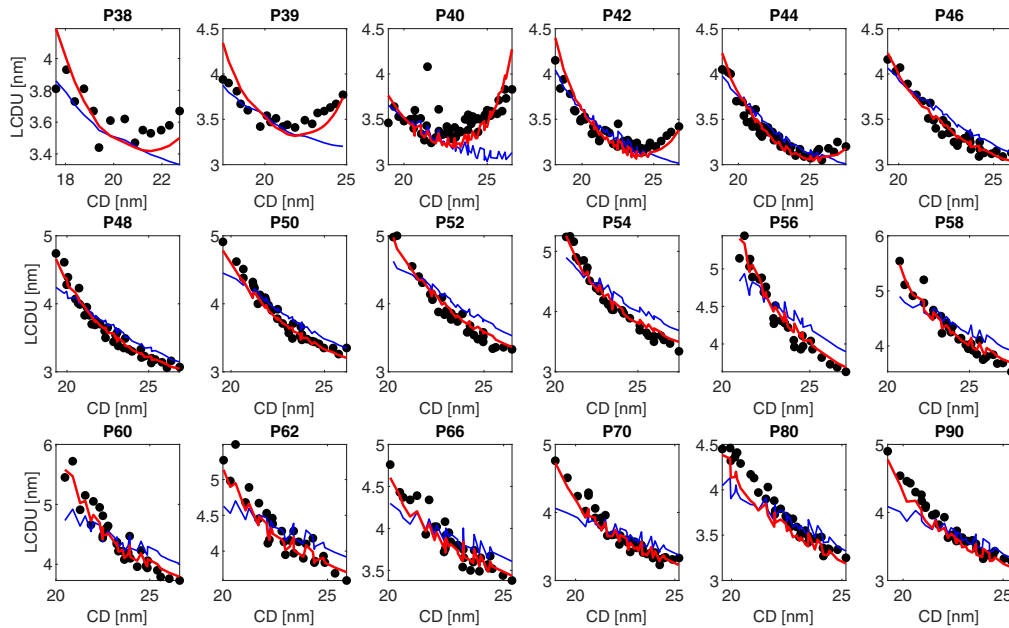
Fig. 21 LCDU (CD) for all of the data in this data set. The symbols are the measured LCDU values (LCDU data obtained from several mask-bias choices; all of these data are plotted together); the red line is the result of the LCDU correlator with optimized cliff terms. (Model parameter: $A = 0.31$, $B = -0.1$ nm, $A_1 = 1.6$ nm, $CD_0 = -2.5$, $CD_1 = 13$ nm). The blue line is the prediction from the best fitting LCDU model without cliff terms.

7 Appendix C. LCDU and Metrology Details

The Appendix describes an argument, based on Prolith simulations, that leads to an expected $\sqrt{CD}$ term in the denominator of the LCDU correlator.

2-D LCDU is more complicated than 1-D LWR, but both cases follow from stochastic line edge roughness (LER). Physically, LER can be thought of as the product of the effective dose noise (EDN) and the local dose sensitivity at the feature edge. To a good approximation, the effective dose and hence EDN are constant around a developed edge. The dose sensitivity can be calculated from the calibrated blurred ILS (ILS_{bl}).[10] Any practical resist process has sufficiently low blur that the opposite feature edges are uncorrelated, so there should be no CD dependence and the quadratic sum leads to the stochastic CD variation (LWR):

$$\mathrm{LWR} = \sqrt{2} * \mathrm{LER} \propto \frac{1}{\mathrm{ILS}_{\mathrm{bl}}}. \qquad (9)$$

In practice, the LER and LWR values are sensitive to the roughness frequency range sampled by the measurement but can be understood by analysis of the PSD curve.

Hole LCDU is similar to LWR if using simple single cut metrology (Fig. 22). The stochastic edge position variation for any edge, 1D or 2D, will depend on local dose sensitivity, and opposite edges should have negligible correlation. But hole metrology is more complicated if an "area-based" or wagon-wheel (WW) method is used as was described in Fig. 2. Multiple independent CD measurements can average out higher frequency variation seen by a single cut. If two diameter measurements are completely uncorrelated (e.g., the H and V cuts in Fig. 22), we would expect hole CD uncertainty to be lowered by $\sqrt{2}$. The amount of LCDU damping associated with area-based hole metrology should increase with both lower edge correlation (low blur) and bigger hole CD.

Quantitatively testing this effect experimentally is difficult, but it can be conveniently done with full physical stochastic simulations. Figure 23(a) shows the expected result: LCDU measured with WW metrology is substantially less than single cut LCDU, and the ratio falls as hole CD increases. A power law fit to these data shows that the CD dependence is ~ -0.55.
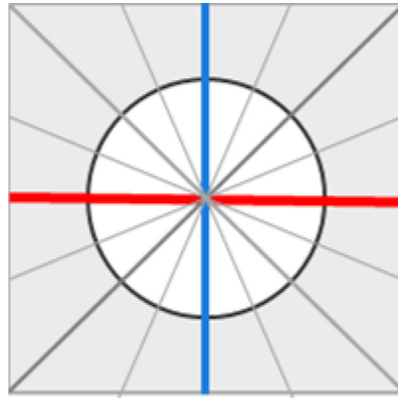
Fig. 22 Single metrology cuts (red horizontal, blue vertical) are highlighted, and additional equally spaced cuts are shown. WW Prolith metrology uses 32 equally spaced cuts (see Fig. 2), but for most resist processes the adjacent cuts give similar information due to edge correlation.
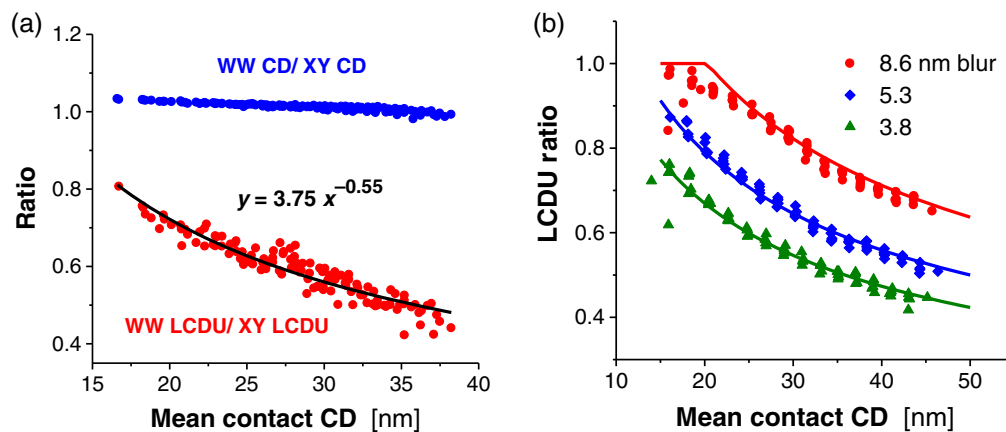

Fig. 23 (a) Analysis of Prolith stochastic simulations showing that the LCDU ratio falls off with increasing hole CD. Calculation details: calibrated CAR, 48-nm pitch square grid holes, reflector mask CD 24 to 34 nm, dose 23 to 44 mJ/cm², fixed focus, 0.33 NA, standard quasar, and 200 stochastic simulations per condition. The WW CD and LCDU numbers use the Prolith area-based metrology method, the XY numbers are the average of the X and Y single cut values. (b) Analysis of Prolith stochastic simulations (points) showing the single parameter model fit (lines). Details: three different CAR models with 72 conditions: square grid hole arrays, 1:1, 1:1.2, 1:2 duty cycles, zero mask bias, 0.33 NA, and quasi-conv illumination. 1000 stochastic simulations per condition at dose-2-size and fixed focus. The LCDU ratio here is the Prolith WW LCDU divided by the average of the single cut LCDUs (X, Y, diag1, diag2).

Figure 23(b) considers the effect in more detail. Here, three different chemically amplified resist models, selected to span a range of blur values, are compared. They show an offset in the calculated metro-dependent LCDU ratios. We expect this effect to be blur-dependent because lower blur implies a lower edge correlation and therefore more effective averaging via the multiple diameter measurements. We expect the reduction in LCDU due to area-based metrology to go as $\sqrt{n}$, where n can be thought of as an effective number of independent hole diameter measurements. The fact that the fit lines nicely overlay the simulation output points verifies this concept and explains the simulation results. In this case, the fit multiplier (m) was found to be 0.42, which implies that the area-based LCDU falls to half the single cut LCDU when CD/blur ~ 10. Also, for small holes with CD $< 2.4 *$ blur, we expect no LCDU reduction due to area-based averaging, round holes, and fixed $n = 1$ as shown in the red curve of Fig. 23(b):

$$LCDU_{ww} = \frac{LCDU_{cut}}{\sqrt{n}}, \tag{10}$$

$$n = \frac{m * CD}{blur}. \tag{11}$$

Note that this analysis indicates that LCDU measured with area-based metrology will have a $1/\sqrt{CD}$ dependence; single cut-measured hole or line-space LCDU or LWR should be CD-independent.

Acknowledgments

References

1. R. Brainard et al., "Shot nose, LER and quantum efficiency of EUV photoresists," *Proc. SPIE* **5374**, 74 (2004).
2. D. Van Steenwinckel et al., "Novel method for characterizing resist performance," *J. Micro/ Nanolith. MEMS MOEMS* **7**(2), 023002 (2008).
3. R. Bristol, "The tri-lateral challenge of resolution, photospeed and LER: scaling below 50 nm?" *Proc. SPIE* **6519**, 65190W (2007).
4. T. Kozawa et al., "Evaluation of chemical gradient enhancement methods for chemically amplified extreme ultraviolet resists," *Jpn. J. Appl. Phys.* **48**, 126004 (2009).
5. J. Biafore et al., "Mechanistic simulation of line-edge roughness," *Proc. SPIE* **6519**, 65190Y (2007).
6. J. Biafore and M. Smith, "Application of stochastic modeling to resist optimization problems," *Proc. SPIE* **8325**, 83250H (2012).
7. P. Naulleau and G. Gallatin, "Line-edge roughness transfer function and its application to determine mask effects in EUV resist characterization," *Appl. Opt.* **42**, 3390 (2003).
8. S.-M. Kim et al., "Understanding stochastic noise," *Proc. SPIE* **9442**, 94420M (2015).
9. O. Yildrim et al., "Improvements in resist performance towards EUV HVM," *Proc. SPIE* **10143**, 101430Q (2017).
10. S. Hansen, "Photoresist and stochastic modeling," *J. Micro/Nanolith. MEMS MOEMS* **17**(1), 013506 (2018).
11. J. Santaclara et al., "One metric to rule them all: new k4 definition for photoresist characterization," *Proc. SPIE* **11323**, 113231A (2020).
12. M. Sanchez et al., "Aerial image contrast using interferometric lithography: effect on line-edge roughness, *Proc. SPIE* **3678**, 160 (1999).
13. H. Koh et al., "Effect of process parameters on pattern edge roughness of chemically-amplified resists," *Proc. SPIE* **3999**, 240 (2000).
14. R. Brainard, J. Cobb, and C. A. Cutler, "Current status of EUV photoresists," *J. Photopolym. Sci. Technol.* **16**, 401 (2003).
15. A. Pawloski et al., "Characterization of line edge roughness in photoresist using an image fading technique," *Proc. SPIE* **5376**, 414 (2004).
16. J. Finders et al., "Contrast optimization for 0.33 NA EUV lithography," *Proc. SPIE* **9776**, 97761P (2016).
17. P. De Bisschop, "Stochastic effects in EUV lithography: random, local CD variability, and printing failures," *J. Micro/Nanolith. MEMS MOEMS* **16**(4), 041013 (2017).

18. J. Van Schoot et al., "High-NA EUV lithography exposure tool: program progress," *Proc. SPIE* **11323**, 1132307 (2020).

19. P. De Bisschop, "Stochastic printing failures in extreme ultraviolet lithography," *J. Micro/ Nanolith. MEMS MOEMS* **17**(4), 041011 (2018).

20. P. De Bisschop and E. Hendrickx, "On the dependencies of the stochastic patterning-failure cliffs in EUVL lithography," *Proc. SPIE* **11323**, 113230J (2020).

21. W. Hinsberg and S. Meyers, "A numeric model for the imaging mechanism of metal oxide EUV resists," *Proc. SPIE* **10146**, 1014604 (2017).

22. R. Bristol and M. Krysak, "Lithographic stochastics: beyond 3σ," *Proc. SPIE* **10143**, 101430Z (2017).

Peter De Bisschop received his PhD in physics from Leuven University, Belgium. He moved to imec in 1986, where he joined the lithography group in 1995. He worked on diverse topics related to exposure-tool-control and -qualification, imaging, masks, rigorous simulations, OPC, and DTCO. His focus in the past few years has been on stochastic effects in EUV.

Steven G. Hansen received his PhD in physical chemistry from the University of California at Berkeley and did postdoctoral work in molecular spectroscopy at Oxford University and Rice University. Since 1990, he has concentrated on photolithography with an emphasis on imaging, simulation, and photoresist.